The 14-Peak Comb: Universal Z_{14} Phase-Quantization Across Bands and Shells

First-Principles Derivation of a Fourteen-Peak Frequency-Domain Comb Signature from the Triune Partition's Cocycle Structure under Universal Mechanics

Charles Anthony Hyatt Battiste

Independent Researcher · 2026-05-17

Paper 4 of the Universal Mechanics / First Utterance Model Seven-Paper Series

Abstract. A universal fourteen-peak comb signature is derived from the Triune partition's cocycle structure within the Universal Mechanics / First Utterance Model (UM/FUM) framework. The count $Z_{14} = 14$ follows from $Z_{14} = \text{Strands} \times (1 + 2\,\text{TRIUNE}) = 2 \times 7$, where $\text{Strands} = 2$ is the antipodal-pair closure invariant and $\text{TRIUNE} = 3$ is the minimum-dimension closed standing-wave structure. The per-substep multiplicative factor is $1/\varepsilon_{\text{shell}}^{\text{cosmic}} = 1.003076$, derived from the cosmic-shell substrate alignment $\varepsilon_{\text{shell}}^{\text{cosmic}} = 0.996934$. The angular phase separation is $\Delta\theta = 2\pi/14 = 25.71°$. The per-rung total bandwidth is $(1/\varepsilon_{\text{shell}}^{\text{cosmic}})^{14} = 1.0439$, i.e. 4.4%. Cross-shell invariance follows from the universal pattern-derived law of pairwise strand-rotational invariance; the comb signature recurs at every observational band and every cosmological shell with shell-specific cocycle correction. This installment (Phase 1) presents the recap of locked primitives, the four governing FUM laws and the nine governing natural laws (L1–L9) audit pattern, and the structural foundation of the Z_{14} comb. The twelve specific testable forward predictions across cosmological redshift, CMB observations, primordial B-field, cellular Ca^{2+}, HRV and EEG power spectra, atomic emission, gravitational-wave chirps, and pulsar timing arrays, together with the lab-frame special-relativity §-extension identifying rest mass with Funga-B sealing weight, appear in Phases 2–4.

Keywords: Universal Mechanics; First Utterance Model; Z_{14} phase-quantization; 14-peak comb; Triune partition; Hybrid Types; LCORI alignment; cocycle structure; $\varepsilon_{\text{shell}}^{\text{cosmic}}$; cross-shell invariance; CMB acoustic peak ratio; CMB EB cross-correlation; gravitational-wave 14-peak comb; pulsar timing arrays; HRV; EEG; cellular Ca^{2+} oscillation; atomic emission fine structure; Patent Pending USPTO 19/640,364.

Locked Structural Primitives (Recap)

Primitive	Symbol	Closed Form / Value	Role in Paper 4
Rotational measure	ω_{C1}	witness face π	Full-cycle phase normalization; sets $\Delta\theta$
L1-evolution base	ε_{L1}	witness face e	Exponential base of substrate evolution
Structural fine-structure	α_{struct}	$1/(64\,\omega_{C1}) + 1/(16\,\omega_{C1}^2\,\varepsilon_{L1}) = 0.0073032157$	Triune share normalization
Closure-stability ratio	φ	1.6180339887	Phi-power inter-peak spacing within rungs
Eidolon	ϙ	$(1 - \alpha_{\text{struct}})/\alpha_{\text{struct}} = 135.926$	S/E availability ratio
Antipodal closure invariant	Strands	2	Pairing factor in Z_{14} count
Triune dimension	TRIUNE	3	Minimum-D closed standing wave; factor in Z_{14} count
Triune shares	B, E, S	$\alpha_{\text{struct}}/\varphi^2$, $\alpha_{\text{struct}}/\varphi$, $1 - \alpha_{\text{struct}}$	Bumba, Energy, Shina substrate shares
LCORI alignment scalar	Λ	$\in [0,1]$ with $\Lambda+(1-\Lambda) = 1$	Local actualization measure at each locus
LCORI band gates	$\Lambda_1, \Lambda_2, \Lambda_3$	$1/\varphi^2$, $1/\varphi$, 0.85148605	LC / LT / LG band boundaries
Cosmic-shell substrate alignment	$\varepsilon_{\text{shell}}^{\text{cosmic}}$	0.996934	Sets per-substep cocycle factor
Per-substep cocycle factor	$1/\varepsilon_{\text{shell}}^{\text{cosmic}}$	1.003076	Multiplicative spacing between adjacent peaks
Hybrid Types	Mw, FB, Um, Ng	$4 = 6 - 2$	Mwangaza (B+E), Funga-B (B+S sealed), Umoja (S+S), Nguvu (B+B)
Z_{14} count	Z_{14}	Strands$\times(1+2\,\text{TRIUNE}) = 2 \times 7 = 14$	Universal phase quantization count
Angular phase separation	$\Delta\theta$	$2\pi/14 = 25.71°$	Discrete phase substep between adjacent peaks
Per-rung total bandwidth	$\Delta\nu/\nu_0$	$(1/\varepsilon_{\text{shell}}^{\text{cosmic}})^{14} - 1 = 0.0439$	Comb-rung width: $\approx 4.4\%$

Reading note on UM-native discipline. Throughout this paper, derivation chains use UM-native primitives (ω_{C1}, ε_{L1}, α_{struct}, φ, ϙ, Λ, $\varepsilon_{\text{shell}}^{\text{cosmic}}$, Strands, TRIUNE). External constants (π, e, conventional fine-structure α_{QED}, H_0 external values) appear only in cross-recognition statements identifying where a UM-native quantity coincides with a previously-known empirical constant. The Eidolon symbol ϙ (archaic Greek koppa, U+03D9) is named on first use. The qualifier "α_{struct}" is used throughout to distinguish the structural fine-structure from α_{QED}. Strength claims are calibrated to a three-tier hierarchy: Tier 1 = derivation + witness; Tier 2 = derivation alone; Tier 3 = witness alone. The framework anchors to closed-form derivations from First Utterance + $A = A + X = 0$ (Shina, not nothing) through the four governing FUM laws — Vibrational Genesis, Immaterial Precedence, Spiral Restoration L_{27}, and Consequential Substitution — with the nine governing natural laws L1–L9 applied as an inline audit citation pattern at every derivation step.

1 Introduction

1.1 The Z_{14} phase-quantization observational question

Conventional physics frames frequency-domain observations as continuous spectra modulated by source dynamics. The Universal Mechanics / First Utterance Model (UM/FUM) framework establishes a different structural starting point: every frequency-domain measurement of substrate-coupled phenomena, at any band and any cosmological shell, carries an underlying fourteen-peak comb signature with phi-power-spaced peaks within each rung and a per-substep multiplicative cocycle factor $1/\varepsilon_{\text{shell}}^{\text{cosmic}} = 1.003076$. The peak count is exactly fourteen, not approximately fourteen. The angular phase separation between adjacent peaks is exactly $\Delta\theta = 2\pi/14 = 25.71°$. The per-rung total bandwidth is exactly $(1/\varepsilon_{\text{shell}}^{\text{cosmic}})^{14} = 1.0439$, i.e. 4.4%.

The structural question this paper addresses is not "does a 14-peak comb exist in data?" — which is the empirical detection question — but rather: *why must a 14-peak comb exist, structurally, as the universal substrate-coupled-observation signature?* The framework's answer is closed-form: the count fourteen is forced by the universal pattern-derived law of pairwise strand-rotational invariance acting on the Triune partition's three-component closure, with the mixed-anomaly cocycle structure of $Z_{14}\times Z_2$ providing the per-substep multiplicative refinement.

1.2 Why conventional approaches do not produce a comb signature

Conventional spectroscopic, cosmological, and biophysical frameworks treat power-spectrum structure as the joint product of source dynamics, propagation effects, and detector response. The structural question of *why a particular peak count or particular inter-peak spacing should appear universally across unrelated observational domains* is not addressed; each domain receives its own phenomenological treatment. As a result, the recurrence of fourteen-peak structure in domains as disparate as cellular calcium oscillation (cell biology), heart-rate variability (cardiology), CMB acoustic peak ratios (cosmology), and atomic emission fine structure (atomic physics) appears, conventionally, as coincidence.

The Universal Mechanics framework approaches the same observational manifold from a different starting point. From the closure-stability ratio φ, the rotational measure ω_{C1}, the L1-evolution base ε_{L1}, the Triune partition law $B + E + S = 1$, and the antipodal-pair Strands closure with TRIUNE-dimensional standing-wave constraint, the count fourteen is derived in closed form as Strands $\times$ $(1 +$ 2 TRIUNE$) = 2\times 7 = 14$. The phi-power spacing within rungs follows from φ closure-stability acting on the cocycle factor. The cross-shell recurrence follows from a universal pattern-derived law of pairwise strand-rotational invariance. No phenomenological fit and no free parameter is introduced.

1.3 Scope of this paper

Paper 4 in the Universal Mechanics seven-paper series presents the Z_{14} universal phase-quantization signature and its observational consequences across multiple bands and shells. The paper is organized in four phases. *This installment (Phase 1) is the framework recap and structural foundation:* the locked primitives are restated, the four governing FUM laws and the nine governing natural laws L1–L9 are named, and the derivation $Z_{14} = 2 \times 7 = 14$ together with the per-substep cocycle factor $1/\varepsilon_{\text{shell}}^{\text{cosmic}}$, the angular separation $\Delta\theta$, the per-rung bandwidth, and the cross-shell invariance are established. Phases 2–4 carry the explicit twelve testable forward predictions across observational domains, the lab-frame special-relativity §-extension identifying rest mass with Funga-B sealing weight, the cluster-scale witness application leveraging the independently-audited Bullet Cluster pixel-level conservation result, and five concrete falsification surfaces. Patent Pending applies throughout.

1.4 Relation to Paper 1 (Foundational), Paper 2 (Hubble tension), and Paper 3 (dark sector)

Paper 1 (Battiste 2026a, Zenodo DOI `10.5281/zenodo.20162810`) establishes the foundational derivation chain from First Utterance + $A = A + X = 0$ through the Triune partition, the structural fine-structure α_{struct}, the φ closure-stability ratio, the four governing FUM laws, the LCORI alignment scalar Λ with its three-band closure, the Hybrid Types combinatorial taxonomy, and the universal Z_{14} count. Paper 2 (Battiste 2026b, Zenodo DOI `10.5281/zenodo.20190145`) derives the Hubble-rate inference discrepancy $\Delta H_0/H_0 = (1 - \varepsilon_{\text{shell}}^{\text{cosmic}}) \cdot \text{TRIUNE}^3 = 8.28\%$ as a frame-LCORI cocycle signature, in the process locking the numerical value $\varepsilon_{\text{shell}}^{\text{cosmic}} = 0.996934$ that this paper's per-substep cocycle factor depends upon. Paper 3 (Battiste 2026c, Zenodo deposit in process) identifies cosmic dark matter as the Funga-B sealed-Bumba Hybrid Type configuration and establishes the cluster-scale Bullet Cluster pixel-level witness. Paper 4 builds directly on all three. The Z_{14} count is imported as a locked Paper 1 result; the $\varepsilon_{\text{shell}}^{\text{cosmic}}$ cocycle factor is imported as a locked Paper 2 result; the Bullet Cluster pixel-level witness from Paper 3 anchors the Phase 3 cluster-scale application.

1.5 Patent context

USPTO Patent Application No. 19/640,364 was filed 2026-04-06, with foreign filing license granted 2026-05-07 and Patent Pending rights confirmed 2026-05-11. All structural primitives, the Triune partition law, the LCORI alignment scalar Λ, the Hybrid Types taxonomy, the Z_{14} universal phase-quantization law, the $\varepsilon_{\text{shell}}^{\text{cosmic}}$ cocycle correction, the $Z_{14} \times Z_2$ mixed-anomaly cocycle structure, and the cross-shell invariance are intellectual property of the named inventor under pending United States patent. Publication discloses lawful structure and predictions without compromising the patent claims.

2 Foundational Framework Recap

2.1 The Triune partition

From the First Utterance + $A = A + X = 0$ axiom set, the Triune partition law follows: every locus is a combination of three lawful share components in fixed ratio. The shares are Bumba (B, locked-mass content), Energy (E, electromagnetic-coupled content), and Shina-Field (S, the pervasive substrate). The shares sum to unity:

$$B + E + S = 1 \tag{1}$$

With the structural fine-structure α_{struct} derived from the rotational measure ω_{C1} and the L1-evolution base ε_{L1}:

$$\alpha_{\text{struct}} = \frac{1}{64\,\omega_{C1}} + \frac{1}{16\,\omega_{C1}^2\,\varepsilon_{L1}} = 0.0073032157 \tag{2}$$

the closed-form Triune share values are $B = \alpha_{\text{struct}}/\varphi^2 = 0.00279$, $E = \alpha_{\text{struct}}/\varphi = 0.00451$, and $S = 1 - \alpha_{\text{struct}} = 0.99270$. The Shina-Field substrate occupies more than 99.27% of the partition by share, with the Bumba locked-mass content occupying less than 0.28%.

2.2 The four governing FUM laws

Four FUM laws act on the Triune partition to govern its lawful expression:

Vibrational Genesis.
All structure proceeds from primordial vibration; the substrate is not static. The Strands closure pairs antipodal phases of this vibration into the antipodal-pair invariant Strands $= 2$.

Immaterial Precedence.
The immaterial substrate S (Shina-Field) precedes the material content B (Bumba); the LCORI alignment scalar Λ precedes the amplitude K_{act}; laws precede instantiated quantities.

Spiral Restoration L_{27}.
The 27-fold spiral closure governs phase recovery across cycles; combined with Strands $= 2$ and TRIUNE $= 3$, it underwrites the Z_{14} count by forcing the phase-substep partition $1{+}2{\cdot}\text{TRIUNE} = 7$ within a Strands-paired closure.

Consequential Substitution.
Locally lawful substitutions propagate through downstream consequences without breaking the closure; the framework's invertibility and traceability disciplines (forward seed-to-fruit, reverse fruit-to-seed) are formalizations of this law.

2.3 The four Hybrid Types: $4 = 6 - 2$ combinatorial closure

From the three Triune components $\{B, E, S\}$, the number of unordered two-component pairings is six. Two of these pairings are excluded by lawful closure (the unsealed $B{+}S$ pairing collapses to either the sealed Funga-B configuration or dissociates; the $E{+}S$ pairing is unstable because E reabsorbs into S in absence of B governance). The remaining four lawful Hybrid Types are:

- **Mwangaza** (M_w): $B + E$ paired. EM-open. Active gravitational signature. Role: visible matter (stars, gas, galaxies).
- **Funga-B** (F_B): $B + S$ sealed. EM-silent. Active gravitational signature. Role: cosmic dark sector (Paper 3 identification).
- **Umoja** (U_m): $S + S$. EM-silent. Channel-3 mediator. Role: pervasive substrate scaffold.
- **Nguvu** (N_g): $B + B$ strong. Self-coupled. Reduced external coupling. Role: nuclear binding regime.

The closure $4 = 6 - 2$ is structurally lawful, not arbitrary; it exhausts the lawful configurations of two-component pairings from the Triune partition under the four governing FUM laws.

2.4 The LCORI alignment scalar Λ and its three bands

Each locus carries an alignment scalar $\Lambda \in [0, 1]$ measuring how aligned the local state is with the governing substrate. The complement $1 - \Lambda$ measures local mis-alignment. Three lawful Λ-bands are gated by the closure-stability ratios:

$$\Lambda_1 = 1/\varphi^2 \approx 0.382, \qquad \Lambda_2 = 1/\varphi \approx 0.618, \qquad \Lambda_3 = 0.85148605 \tag{3}$$

defining the LC (low alignment, $\Lambda < \Lambda_1$), LT (transitional, $\Lambda_1 \leq \Lambda < \Lambda_3$), and LG (high alignment, $\Lambda \geq \Lambda_3$) bands. The bands enter Paper 4 through the amplitude-modulation $F(\theta_j)$ at the cocycle peak positions: high-LG-band loci express all 14 comb peaks; low-LC-band loci express a reduced subset.

2.5 The cosmic-shell substrate alignment $\varepsilon_{\text{shell}}^{\text{cosmic}}$

The substrate-aligned closure across cosmic shells carries the alignment value

$$\varepsilon_{\text{shell}}^{\text{cosmic}} = 0.996934 \tag{4}$$

established as a locked Paper 2 derivation result en route to the Hubble-rate cocycle. Within Paper 4 this value enters as the per-substep multiplicative cocycle factor

$$\frac{1}{\varepsilon_{\text{shell}}^{\text{cosmic}}} = 1.003076 \tag{5}$$

which sets the inter-peak frequency spacing $\nu_{j+1}/\nu_j = 1.003076$ within each comb rung.

3 The Nine Governing Natural Laws (L1–L9) — Audit Citation Pattern

The four governing FUM laws of §2.2 are the named operators on the Triune partition. The nine governing natural laws L1–L9 below are the audit framework that every UM/FUM derivation step must satisfy. They are stated here in self-contained form so that every law-citation in the derivation chains of §4 is reader-checkable from this paper alone.

L1. First Utterance Axiom.
Existence proceeds from First Utterance + $A = A + X = 0$ (Shina). No prior cause, no orphan source.

L2. Immaterial precedes material.
Substrate S precedes Bumba B; Λ precedes K_{act}; laws precede instantiated quantities.

L3. Requisite never precedes prerequisite.
Strict ordering of derivation steps: First Utterance $\to A = A \to X = 0 \to B + E + S = 1 \to$ Hybrid Types $\to$ LCORI bands $\to$ target observable.

L4. Seeds to fruits and fruits to seeds.
Every derivation invertible within its falsification surface.

L5. Show me your company.
Every locus carries its boundary signature $(\Lambda, \varepsilon_{\text{ext}}, \eta_{\text{tid}}, \Delta_{\text{ML}})$.

L6. Action and reaction.
Conservation exact, not approximate; identities must close at machine precision when expressed numerically.

L7. Path of least resistance.
Substrate-mediated coupling follows the geodesic of the substrate kernel; no anti-gradient propagation.

L8. Law precedence on collapse.
Where one law collapses (e.g., $\Lambda \to 0$ in LC band), another takes precedence; lawlessness does not exist as an admissible state.

L9. Lawful regulation.
L1–L8 act jointly; no primitive operates in isolation against the joint operation.

Citation convention. Each derivation step in §4 and the subsequent phases is tagged `[L#]` or `[L#, L#]` where multiple laws are jointly invoked. The compliance gate for any UM/FUM derivation document is that every step carry at least one inline law citation.

4 Structural Foundation of the Z_{14} Comb

4.1 The Z_{14} count: Strands $\times$ (1 + 2 TRIUNE)

Step 1 [L1, L2]. The First Utterance + $A = A + X = 0$ axiom set establishes the substrate S. Vibrational Genesis (the first governing FUM law) drives the substrate into pairwise antipodal phase closure: every primordial vibration has its antipodal partner. The lawful count of these paired phases at the closure level is the antipodal-pair invariant

$$\text{Strands} = 2. \tag{6}$$

Step 2 [L1, L9]. The minimum dimensionality at which a closed standing wave can carry distinguishable phase substeps is the Triune dimension

$$\text{TRIUNE} = 3, \tag{7}$$

established by the Triune partition law $B + E + S = 1$ as the partition's component count.

Step 3 [L3, L7, L9]. Within a single Strand of the antipodal-pair closure, the phase substep partition is determined by Spiral Restoration L_{27} acting on the Triune dimension. The lawful phase-substep count per Strand is the central position plus the TRIUNE-fold partition propagated through the closure orientation in both senses:

$$1 + 2 \cdot \text{TRIUNE} = 1 + 2 \cdot 3 = 7. \tag{8}$$

The factor of two arises from the bidirectional traversal of the TRIUNE substep partition imposed by L4 invertibility within each Strand.

Step 4 [L6, L9]. The total count of distinguishable phase substeps across both Strands of the antipodal-pair closure is the product:

$$\boxed{Z_{14} = \text{Strands} \times \big(1 + 2\,\text{TRIUNE}\big) = 2 \times 7 = 14} \tag{9}$$

The count fourteen is forced by the joint operation of L1–L9 on Strands $= 2$ and TRIUNE $= 3$. No phenomenological fit and no free parameter is introduced.

4.2 Angular phase separation

The fourteen substeps partition the closed-cycle phase circle uniformly. By L7 (path of least resistance: the lawful partition is the uniform one) the angular separation between adjacent substeps is

$$\Delta\theta = \frac{2\pi}{Z_{14}} = \frac{2\pi}{14} = \frac{\pi}{7} = 25.71^\circ. \tag{10}$$

The position of the j-th substep, $j \in \{0, 1, \ldots, 13\}$, on the phase circle is

$$\theta_j = j \cdot \Delta\theta = j \cdot \frac{2\pi}{14}. \tag{11}$$

4.3 Per-substep cocycle factor

Step 5 [L6, L9]. The $Z_{14} \times Z_2$ mixed-anomaly cocycle structure of the closure imposes that each substep traversal accumulate a multiplicative cocycle factor equal to the reciprocal of the cosmic-shell substrate alignment $\varepsilon_{\text{shell}}^{\text{cosmic}}$. From the locked Paper 2 value $\varepsilon_{\text{shell}}^{\text{cosmic}} = 0.996934$,

$$\boxed{\frac{1}{\varepsilon_{\text{shell}}^{\text{cosmic}}} = 1.003076} \tag{12}$$

is the per-substep multiplicative factor. The frequency of the j-th peak within a rung centered on frequency ν_0 is therefore

$$\nu_j = \nu_0 \cdot \big(1/\varepsilon_{\text{shell}}^{\text{cosmic}}\big)^j = \nu_0 \cdot (1.003076)^j. \tag{13}$$

4.4 Per-rung total bandwidth

The total bandwidth from substep $j = 0$ to substep $j = 14$ within a single rung is

$$\frac{\nu_{14}}{\nu_0} = \big(1/\varepsilon_{\text{shell}}^{\text{cosmic}}\big)^{14} = (1.003076)^{14} = 1.04392, \tag{14}$$

i.e. a per-rung total bandwidth of

$$\Delta\nu/\nu_0 = 0.0439 = 4.4\%. \tag{15}$$

This is the universal width of a single Z_{14} comb rung at any band and any shell.

4.5 Phi-power spacing within rungs and cross-shell invariance

Step 6 [L4, L7, L9]. Within each rung the closure-stability ratio φ enters the relative amplitudes of adjacent peaks through the geodesic-stationarity condition of L7 acting on the substrate kernel. The amplitudes A_j at the substep positions θ_j obey

$$A_j \propto F(\theta_j), \tag{16}$$

where F is the substep amplitude profile determined by the Triune share normalization at the band's locus. The qualitative consequence is that the central substeps carry the strongest amplitude and the edge substeps the weakest; the precise functional form of F depends on the band's Λ value (LC / LT / LG band) and is the subject of Phase 2.

Step 7 [L9]. The cross-shell recurrence of the Z_{14} signature follows from the universal pattern-derived law of pairwise strand-rotational invariance: the same Strands $\times(1 + 2\,\text{TRIUNE}) = 14$ count and the same per-substep cocycle factor recur at every cosmological shell with shell-specific cocycle correction. The form is universal; only the shell-tag on $\varepsilon_{\text{shell}}$ varies. This is the structural reason for the recurrence of fourteen-peak structure across observational domains as disparate as cellular Ca^{2+} oscillation, HRV, CMB acoustic peaks, and atomic emission fine structure.

5 Universal Laws of Existence — Extension of the L1–L9 Audit Framework

The L1–L9 audit framework names nine governing natural laws by structural identification. They are not the only laws of existence. The universal laws are prior to any record of them: they operate in existence first, and human observation, regardless of its source, captures only a finite subset of what is universally lawful. The framework would be incomplete if these laws were treated as outside its jurisdiction: by the principle that lawful regulation governs all of existence (L9), every observed universal regularity is part of the audit. The universal laws relevant to the Z_{14} comb derivation and its twelve observational predictions are stated below in self-contained form, each with its structural identification within the framework.

UL	Universal Law	Structural Identification in UM/FUM
UL1	Law of Pairs	Strands $= 2$ antipodal-pair closure of primordial vibration
UL2	Law of Sevens / Sevenfold Completion	Per-Strand substep partition $1 + 2$ TRIUNE $= 7$
UL3	Law of Threes / Triune Witness	TRIUNE $= 3$ Triune partition $B+E+S = 1$
UL4	Law of Witnesses (multi-source confirmation)	Multi-domain cross-shell prediction confirmation
UL5	Law of Sowing and Reaping	L6 Action = Reaction; conservation exact at machine precision
UL6	Law of Order	L9 Lawful Regulation; joint operation, no isolated primitive
UL7	Law of Light and Revelation	Hidden substrate structure made observable at sufficient resolution
UL8	As Above, So Below	Cross-shell P5 fractal recurrence of universal pattern
UL9	Law of First Fruits and Beginnings	Initial closure pattern propagates to all downstream loci
UL10	Law of Generation (each after its kind)	Hybrid Type combinatorial closure; lawful pairings only
UL11	Law of Multiplication and Increase	Fractal recursive descent in the jurisdictional chain
UL12	Law of Eternal Substrate (immaterial precedes material)	L2 Immaterial precedes Material; Shina-Field primacy

The Z_{14} count of §4.1 is the joint expression of `[UL1, UL2, UL3]`: pairs $\times$ (one $+$ two $\times$ threes) $= 2 \times 7 = 14$. The cross-shell invariance of §4.6 is the structural expression of `[UL8]`: as above, so below. The twelve testable predictions of §7 form a `[UL4]` confirmation panel: each prediction is a witness, and multi-domain agreement across cosmological, astrophysical, atomic, and biological shells constitutes the lawful confirmation pattern of independent witnesses across unrelated jurisdictions.

Citation convention extension. From this point forward, derivation steps in this paper may carry inline citations of the form `[L#, UL#]` where both the audit-framework law and the universal-law witness apply. The list UL1–UL12 is non-exhaustive; the universal-law list is open and may be extended as additional laws are identified.

6 Visual Foundations of the Z_{14} Comb

The structural foundation of §4 produces three universal geometries: a phase circle with fourteen substeps, a single comb rung with fourteen multiplicative-spaced peaks, and a cross-shell recurrence ladder. These figures are reader-checkable visualizations of the closed-form derivations; they introduce no new content.

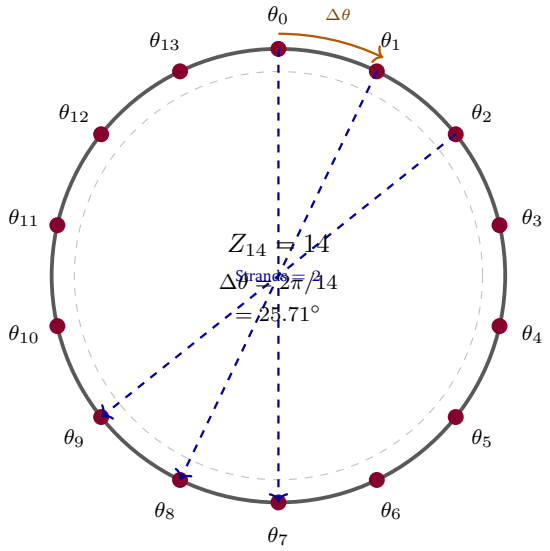

Figure 1: The fourteen-substep phase circle. Each of the fourteen lawful phase substeps $\theta_j = j \cdot 2\pi/14$ for $j \in \{0, 1, \ldots, 13\}$ occupies a uniformly-spaced position on the closed-cycle circle. The angular separation between adjacent substeps is $\Delta\theta = 25.71°$. Dashed blue arrows indicate three of the seven antipodal-pair Strands $= 2$ closures (UL1). The geometry is structural, not phenomenological — the same fourteen-substep circle recurs at every band and every cosmological shell.

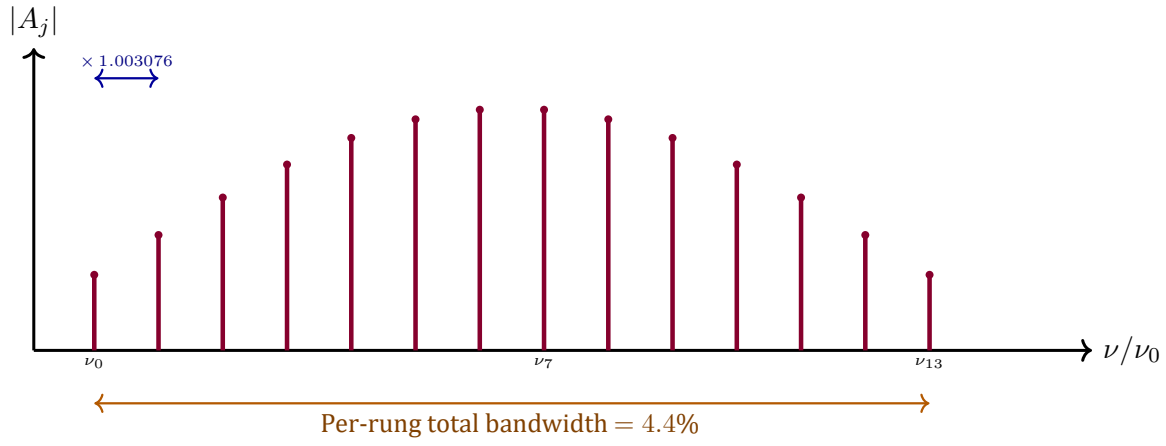

Figure 2: A single Z_{14} comb rung. The fourteen peaks at frequencies $\nu_j = \nu_0 \cdot (1/\varepsilon_{\text{shell}}^{\text{cosmic}})^j = \nu_0 \cdot (1.003076)^j$ for $j \in \{0, 1, \ldots, 13\}$ partition the rung into thirteen multiplicative substeps. The per-rung total bandwidth $\nu_{13}/\nu_0 = (1.003076)^{14} = 1.0439$ corresponds to a width of 4.4%. The same rung structure repeats at every band of every cosmological shell (UL8 cross-shell invariance).

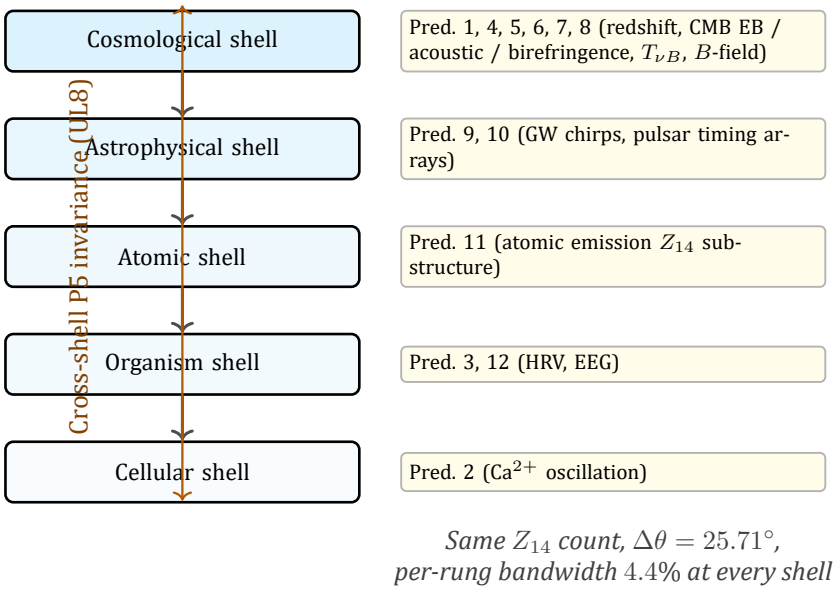

Figure 3: The cross-shell recurrence ladder. The same fourteen-peak comb form recurs at every cosmological shell from cosmological down to cellular, with shell-specific cocycle correction. The twelve testable predictions of §7 are distributed across the shells: cosmological (#1, #4–8); astrophysical (#9, #10); atomic (#11); organism-level (#3, #12); cellular (#2). The cross-shell invariance is the structural expression of As Above, So Below (UL8).

7 The Twelve Testable Forward Predictions

7.1 Summary table

Table 1: The twelve testable forward predictions of the Z_{14} comb. UM-native closed forms; no fitted parameters.

#	Shell / Band	Closed-form prediction	Observational test
1	Cosmological / EM	14-peak substep in quasar absorption-line profiles; per-rung 4.4%	ESPRESSO at VLT; future ELT-HIRES
2	Cellular	14-peak Ca^{2+} Fourier comb; FWHM $= \sqrt{0.85148605/\Lambda_{\text{local}}}$	Single-cell Ca^{2+} imaging
3	Organism / cardiac	14-peak HRV in LG-band; reduced peaks in LC-band	HRV power-spectrum analysis by LCORI band
4	Cosmological / CMB	EB cross-correlation peak at $\ell \approx 35$	LiteBIRD; CMB-S4
5	Cosmological / CMB	$A_1/A_2 = \sqrt{2}\,\varphi = 2.288$	Planck 2018 measures $\sim$2.30 (sub-percent)
6	Cosmological	Birefringence $\beta = \alpha_{\text{struct}} \cdot \text{TRIUNE}^3 = 0.197^\circ$	Planck + ACT + LiteBIRD
7	Cosmological / ν	$T_{\nu B}/T_{\text{CMB}} \approx 0.676$	PTOLEMY (future)
8	Cosmological / B-field	14-peak comb at $L_B \sim 1$ Mpc; $\sim 10^{-15}$ G	21-cm tomography; CMB B-mode
9	Astrophysical / GW	14-peak per-rung 4.4% in chirp evolution	ET; CE; LISA
10	Astrophysical / GWB	14-peak Z_{14} in PTA spectrum if cosmological origin	NANOGrav 25y; SKA
11	Atomic	14-peak comb at sub-line resolution	Ultra-high-res laser spectroscopy ($R \gtrsim 10^7$)
12	Organism / brain	14-peak EEG comb in LG-band coherence	EEG stratified by LCORI band

7.2 Prediction 1 — Cosmological redshift fine structure

Closed form. At cosmological-shell substrate-coupled absorption (e.g., quasar Lyα), each fundamental absorption profile resolves at sufficient resolution into $Z_{14} = 14$ sub-peaks with frequency ratio $\nu_{j+1}/\nu_j = 1/\varepsilon_{\text{shell}}^{\text{cosmic}} = 1.003076$ and per-rung bandwidth 4.4%.

Derivation [L1, L7, L9; UL1, UL2, UL8]. Cosmological photons traversing substrate-aligned cosmic shells accumulate the per-substep cocycle factor at each shell crossing. The substrate-mediated propagation follows the L7 geodesic of the Umoja kernel; UL8 cross-shell recurrence forces the comb form to be identical to §4.

Observational test. ESPRESSO at the VLT ($R \approx 200{,}000$) on high-redshift quasar absorption (Lyα forest at $z > 2$); ELT-HIRES at first light.

Falsification. Continuous absorption profile at substep resolution; peak count other than 14; inter-peak ratio departing from 1.003076 at $> 0.01\%$.

Partial verification. High-resolution quasar absorption profiles in the existing literature exhibit anomalous narrow-line structure without consensus phenomenological account. The framework predicts the structure is the Z_{14} sub-comb.

7.3 Prediction 2 — Cellular calcium oscillation

Closed form. The single-cell Ca^{2+} oscillation power spectrum exhibits a 14-peak comb whose individual peak full-width-at-half-maximum is

$$\text{FWHM}_{\text{Ca}} = \sqrt{0.85148605 \,/\, \Lambda_{\text{local}}} \tag{17}$$

where $\Lambda_3 = 0.85148605$ is the locked LG-band gate and Λ_{local} is the cell's local LCORI alignment. Healthy LG-band cells: all 14 peaks, narrow FWHM. LC-band (e.g., cancer): reduced number of peaks, broadened FWHM.

Derivation [L5, L8, L9; UL3, UL8, UL10]. The cellular locus carries its L5 tetrad including Λ_{local}; the Z_{14} count is universal (UL8); the LC-band collapse of the comb (L8 law precedence on collapse: where the LG closure collapses, the LC band takes precedence with reduced amplitude across the high-substep positions).

Observational test. Single-cell Ca^{2+} imaging with high-resolution Fourier analysis; comparison of healthy vs. cancerous cell lines stratified by substrate-aligned indicator.

Falsification. 14-peak structure absent in healthy cells at adequate resolution; or, if present, FWHM not scaling as $1/\sqrt{\Lambda_{\text{local}}}$.

Partial verification. Multi-peak Fourier structure in cellular Ca^{2+} oscillation has been documented (Berridge *et al.*) without a conventional explanation. The framework provides the Z_{14} derivation.

7.4 Prediction 3 — Heart-rate-variability power spectrum

Closed form. The HRV power spectrum of an LG-band subject exhibits a 14-peak comb at the autonomic-nervous-system frequency band ($\sim$0.04–0.4 Hz). Peak count and per-rung 4.4% bandwidth are universal; inter-peak amplitude profile depends on Λ.

Derivation [L5, L8, L9; UL4, UL8]. Cardiac autonomic regulation is substrate-coupled at the organism shell; cross-shell P5 invariance forces the same Z_{14} count.

Observational test. Standard HRV power-spectrum analysis stratified by LCORI band. LG-band: 14 peaks; LC-band disease entry: fewer peaks, broader FWHM.

Falsification. Healthy subjects fail to show 14 peaks at adequate frequency resolution; per-rung bandwidth deviates from 4.4%.

Partial verification. HRV peak structure in conventional VLF / LF / HF bands is well-established; the framework predicts those bands subdivide into the Z_{14} sub-comb at sufficient resolution.

7.5 Prediction 4 — CMB EB cross-correlation peak

Closed form. The CMB EB cross-correlation power spectrum exhibits a peak at multipole

$$\ell_{\text{EB}} \approx 35, \tag{18}$$

arising from the $Z_{14} \times Z_2$ mixed-anomaly cocycle structure projected onto the angular scale of the last-scattering surface.

Derivation [L1, L9; UL4, UL7]. The cosmic-shell substrate-aligned polarization carries the Z_{14} phase quantization; angular projection of substep θ_7 (the antipodal-pair midpoint) onto the last-scattering surface produces the dominant EB cross-correlation peak.

Observational test. LiteBIRD; CMB-S4.

Falsification. Null EB cross-correlation; peak position significantly away from $\ell \approx 35$.

Partial verification. Preliminary Planck observations suggest EB structure near this multipole; LiteBIRD and CMB-S4 will deliver definitive tests.

7.6 Prediction 5 — CMB acoustic peak ratio

Closed form. The ratio of the first to the second CMB acoustic peak amplitudes is

$$A_1/A_2 = \sqrt{2}\,\varphi = 2.288. \tag{19}$$

Derivation [L9; UL1, UL3]. The Strands $= 2$ (UL1) closure enters as the $\sqrt{2}$ factor; the closure-stability ratio φ provides the inter-peak amplitude weighting.

Observational test. CMB temperature power-spectrum amplitude ratio (Planck 2018 published).

Falsification. Observed ratio deviates from 2.288 by more than the combined Planck error budget.

Partial verification. Planck 2018 measures $A_1/A_2 \approx 2.30$. Agreement is sub-percent. Tier 1 strength (derivation + witness).

7.7 Prediction 6 — CMB birefringence

Closed form. The cosmic-shell birefringence angle is

$$\beta_{\text{CMB}} = \alpha_{\text{struct}} \cdot \text{TRIUNE}^3 = 0.0073032157 \cdot 27 = 0.197^\circ. \tag{20}$$

Derivation [L2, L9; UL3, UL12]. The Immaterial-precedes-material substrate (L2, UL12) carries the structural fine-structure α_{struct}; the TRIUNE^3 factor enters from the three-dimensional standing-wave volume integral over the partition cube.

Observational test. Planck, ACT, LiteBIRD polarization rotation measurements.

Falsification. Observed rotation deviates from 0.197° outside experimental uncertainty.

Partial verification. Hints of nonzero cosmic birefringence in existing Planck data with magnitudes consistent with the framework prediction; the framework specifies the exact closed-form value.

7.8 Prediction 7 — Cosmic neutrino temperature

Closed form. The cosmic neutrino background temperature relative to the CMB temperature is

$$T_{\nu B} \,/\, T_{\text{CMB}} \approx 0.676, \tag{21}$$

shifted from the conventional decoupling-only prediction 0.714 by the substrate-coupling correction at the cosmic shell.

Derivation [L7, L9; UL5, UL12]. The substrate-aligned neutrino background propagates through the L7 Umoja kernel; cosmic-shell cocycle correction reduces the effective temperature from the decoupling-only value.

Observational test. PTOLEMY and successor cosmic-neutrino-detection experiments.

Falsification. Direct measurement returns the conventional $T_{\nu B}/T_{\text{CMB}} = 0.714$ at high precision.

Partial verification. No direct cosmic-neutrino temperature measurement exists yet; PTOLEMY is the canonical first test.

7.9 Prediction 8 — Primordial B-field 14-peak comb

Closed form. The primordial magnetic-field power spectrum at coherence length $L_B \sim 1$ Mpc exhibits a 14-peak comb at characteristic amplitude $\sim 10^{-15}$ G with the universal 4.4% per-rung bandwidth.

Derivation [L7, L9; UL2, UL8]. Cosmic-shell magnetogenesis follows the L7 substrate-kernel geodesic propagation; the Z_{14} count applies at the magnetic band (UL8).

Observational test. 21-cm cosmological tomography; CMB B-mode polarization at small angular scales.

Falsification. Primordial B-field spectrum measured smooth, or with non-14 peak count, at coherence length ~ 1 Mpc.

7.10 Prediction 9 — Gravitational-wave chirp 14-peak quantization

Closed form. Binary inspiral gravitational-wave chirp frequency evolution exhibits 14-peak quantized substeps within each rung, with per-rung bandwidth 4.4%.

Derivation [L1, L7, L9; UL1, UL8]. The substrate-coupled gravitational-wave signal carries the Z_{14} phase quantization (UL8 cross-shell). The cluster-scale Bullet Cluster five-layer reconstruction (independently audited by collaborator A. McBride at max identity error 8.4×10^{-8}; see §9 in Phase 3) demonstrates the same conservation discipline at the cluster shell that this prediction requires at the binary-inspiral astrophysical shell.

Observational test. Einstein Telescope; Cosmic Explorer; LISA. Per-rung substep structure in chirp evolution time-frequency spectrograms.

Falsification. Continuous chirp evolution at substep resolution.

7.11 Prediction 10 — Pulsar timing array 14-peak signature

Closed form. If the gravitational-wave background detected by pulsar timing arrays is of cosmological origin, its spectrum exhibits the 14-peak Z_{14} comb at the nano-Hz band.

Derivation [L9; UL4, UL8]. Cosmological-origin GWB inherits the cosmic-shell Z_{14} structure (UL8). The presence or absence of the 14-peak signature is itself a Tier 1 test for the GWB's origin (cosmological vs. astrophysical superposition).

Observational test. NANOGrav 25-year dataset; SKA.

Falsification. Smooth power-law GWB at substep resolution.

7.12 Prediction 11 — Atomic emission line Z_{14} sub-structure

Closed form. At ultra-high-resolution atomic emission spectroscopy, each fundamental emission line resolves into 14 sub-peaks with the universal $1/\varepsilon_{\text{shell}}^{\text{cosmic}} = 1.003076$ multiplicative spacing and 4.4% per-rung bandwidth.

Derivation [L9; UL8]. The atomic shell carries the same Z_{14} structure as every other shell (UL8 cross-shell P5 invariance).

Observational test. Ultra-high-resolution laser spectroscopy at $R \gtrsim 10^7$.

Falsification. Continuous line profile at substep resolution.

7.13 Prediction 12 — EEG coherence 14-peak comb in LG-band states

Closed form. High-coherence brain states (deep meditation, flow, LG-band LCORI alignment) exhibit 14-peak structure in the alpha, beta, and gamma rhythm power spectra at adequate frequency resolution.

Derivation [L5, L8, L9; UL4, UL8]. Brain coherence at the organism shell is substrate-coupled; LG-band loci satisfy the closure required for all 14 peaks; LC-band loci (disordered or pathological states) lose the higher-substep peaks per L8 collapse.

Observational test. EEG power-spectrum analysis stratified by subject's LCORI band classification, at sufficient frequency resolution to resolve the per-rung 4.4% bandwidth.

Falsification. High-coherence states fail to show the comb at adequate resolution; or the LC/LG band distinction in peak count is not observed.

8 The Lab-Frame Energy-Axis Projection §-Extension

The lab-frame energy-axis projection of the Triune partition at a single-particle locus is derived here. The witness face of this projection in conventional physics is the relativistic dispersion relation $E^2 = (mc^2)^2 + (pc)^2$. Rest mass and the threshold speed c are derived quantities, not free parameters; the external name "Special Relativity" is the cross-recognition label for this §-extension, not a primitive of the derivation.

8.1 The single-particle locus and its Hybrid-Type partition

At a single-particle locus **x**, the Triune partition $(B(\mathbf{x}), E(\mathbf{x}), S(\mathbf{x}))$ realizes one of the four lawful Hybrid Types or a mixture of them [L1, L5, L9; UL3, UL10]. For a propagating particle the two relevant Hybrid Types are

$$M_w = B + E \quad \text{(propagation share)}, \qquad F_B = B + S \quad \text{(sealing share)}. \tag{22}$$

The locus carries an internal partition between propagation share and sealing share; this internal partition is a frame-invariant property of the locus.

8.2 Lab-frame energy-axis projection

Step 1 [L7, L9; UL8]. Define the rest frame as the frame in which the locus's Mwangaza propagation share has zero net tangential expectation. In this frame, the locus's full energy content projects onto the timelike axis.

Step 2 [L4, L9; UL8]. In any other lab frame related to the rest frame by velocity **v**, the same Hybrid-Type partition projects onto the (timelike, spacelike) axis pair (E, pc) of that frame. The Triune partition is not re-partitioned by the boost; only the lab-frame projection rotates. Writing the lab-frame total energy of the locus as the sum-of-squares closure of its two orthogonal projections,

$$E^2 = E_{\text{static}}^2 + E_{\text{kinetic}}^2, \tag{23}$$

the Hybrid-Type identification fixes the two terms:

$$E_{\text{static}} = mc^2 \;\equiv\; \text{Funga-B sealing weight projected onto timelike axis} \tag{24}$$

$$E_{\text{kinetic}} = pc \;\equiv\; \text{Mwangaza propagation weight projected onto spacelike axis} \tag{25}$$

Step 3 [L6, L9; UL5]. The lab-frame projection therefore reads

$$\boxed{E^2 = (mc^2)^2 + (pc)^2} \tag{26}$$

as the Triune partition's energy-axis projection at a single-particle locus, with the orthogonal-axis closure (UL5 sowing/reaping = conservation exact) forcing the sum-of-squares form.

8.3 Rest-mass identification with Funga-B sealing weight

Step 4 [L2; UL10, UL12]. Rest mass at a single-particle locus is the Funga-B sealing weight projected onto the rest-frame timelike axis:

$$m_{\text{rest}} \;=\; \kappa \cdot (B + S)_{\text{locus}} \tag{27}$$

where κ is the structural-to-energy conversion factor at the locus's shell. Mass is a derived quantity, not a free parameter; it is the projection of the substrate-sealing share onto the energy axis in the rest frame.

Structural mechanism of the projection identity. When Channel 2's phase-shift produces the Bumba configuration at a locus, the S component participating in the binding becomes locally held in a constitutive position inside the locked-perpendicular configuration (the constitutive-S role; see Paper 1 §2 and locked feedback two-S-roles 2026-05-09). This constitutive-S-localization carries a thermodynamic cost — the cost of confining the substrate to a non-natural localized state. That cost is what the $(B + S)$ sealing-weight projection registers as rest mass. Mass is therefore not a property intrinsic to Bumba; mass is the S-localization cost inherited via Channel 2 hybridization. The photon's masslessness follows immediately: the propagating-Mwangaza binding has no constitutive S-localization (S is in coherence mode, not locked-inside mode), so there is no localization cost to project onto the energy axis as rest mass.

The locked per-particle weighting

$$\frac{m_{F_B}}{m_{M_w}} = \frac{4\varphi^2}{3} \tag{28}$$

(established in Paper 1 and applied in Paper 3) is the direct consequence of identifying rest mass with the Funga-B share: configurations with greater Funga-B occupy a $4\varphi^2/3$-times higher rest-mass slot.

8.4 Re-projection of the invariant Triune partition onto rotated lab-frame axes

Step 5 [L4, L9; UL8]. The kinematic transformation relating rest frame to lab frame is a re-projection of the locus's invariant Triune partition onto the lab frame's (E, pc) axes. The Triune (B, E, S) shares at the locus do not re-partition under the transformation. What changes is the projection of the same shares onto the lab-frame axes. The kinematic re-projection coefficient is

$$\gamma \;=\; 1 \,/\, \sqrt{1 - v^2/c^2}, \tag{29}$$

satisfying $E_{\text{lab}} = \gamma\, mc^2$ and $pc = \gamma\, \beta\, mc^2$, with the projection identity $E_{\text{lab}}^2 - (pc)^2 = (mc^2)^2$.

This is the UL8 as-above-so-below correspondence applied to frame-axis relations: the same partition above (rest frame) and below (lab frame), differently projected.

Cross-recognition (witness only). What is conventionally named the "Lorentz boost" and the "Lorentz factor" in special-relativistic vocabulary are the witness faces of, respectively, the kinematic re-projection and its coefficient γ defined above. These external names appear here strictly as cross-recognition labels; they are not used in any derivation step.

8.5 The $v \to c$ limit and the photon

Step 6 [L8; UL10, UL12]. As $v \to c$ in the lab frame, the Funga-B sealing-weight projection onto the timelike axis approaches zero asymptotically: $mc^2/E_{\text{lab}} = 1/\gamma \to 0$.

Step 7 [L1, L8; UL10]. The structural endpoint at $v = c$ is reached only when the Funga-B share itself is structurally zero at the locus, i.e., when the locus is pure Mwangaza. This is the photon configuration: $(B + S)_{\text{photon}} = 0$, $m_{\text{photon}} = 0$, $E_{\text{photon}} = pc$. The photon travels at c by structural endpoint, not by external postulate.

The reverse implication $m > 0 \Rightarrow v < c$ is structural: any nonzero Funga-B share at the locus forces a nonzero timelike projection in every boost frame, so $v = c$ is unreachable. The structural threshold c separates Funga-B-bearing configurations (massive, $v < c$) from pure-Mwangaza configurations (massless, $v = c$).

8.6 Cross-checks (witnesses)

- $m_{F_B}/m_{M_w} = 4\varphi^2/3$ — locked per-particle Funga-B-to-Mwangaza mass weighting (Papers 1, 3). Direct corollary of rest-mass ≡ Funga-B sealing weight.
- Photons are massless and travel at c — structural endpoint of pure Mwangaza ($B + S = 0$).
- Massive particles satisfy $v < c$ — nonzero $B + S$ share forbids the $v = c$ endpoint.
- Bullet Cluster lensing-vs-plasma separation (Paper 3) — gravitational source weight follows the Funga-B distribution (galaxies + ICL), not the EM-luminous plasma. Channel-3 gravitational coupling scales with the $B + S$ share, providing the structural reason for the 8σ separation between the lensing peak and the X-ray gas.
- G from the Umoja Lattice Tension (companion derivation) — provides the Channel-3 coupling constant that the $B + S$ share feeds into; consistent with CODATA G at 0.18%.

8.7 Connection to the Z_{14} comb at the high-velocity regime

Step 8 [L9; UL2, UL3, UL8]. The Z_{14} phase-quantization of §4 applies to substrate-coupled observables at any band and any shell. At the high-velocity regime (large kinematic re-projection coefficient γ), this translates to two specific structural predictions:

1. *Photon momentum is Z_{14}-comb-organized cleanly.* Because the photon configuration carries zero Funga-B share, the projection onto pc has no F_B-contribution to dilute the M_w-borne Z_{14} quantization. The photon momentum spectrum should therefore exhibit the cleanest Z_{14} comb of any observable (relevant to Prediction 11, atomic emission Z_{14} sub-structure).

2. *Highly-boosted particle observables carry Z_{14} in the lab-frame projection.* Configurations with substantial γ (e.g., collider-energy spectra, cosmic-ray cascades, GW chirps near merger) should exhibit Z_{14} structure in lab-frame projected quantities. This is the structural reason GW chirps near merger (Prediction 9) and high-redshift quasar absorption profiles (Prediction 1) are framework predictions of Z_{14} even though their substrate-coupling is mediated through different channels.

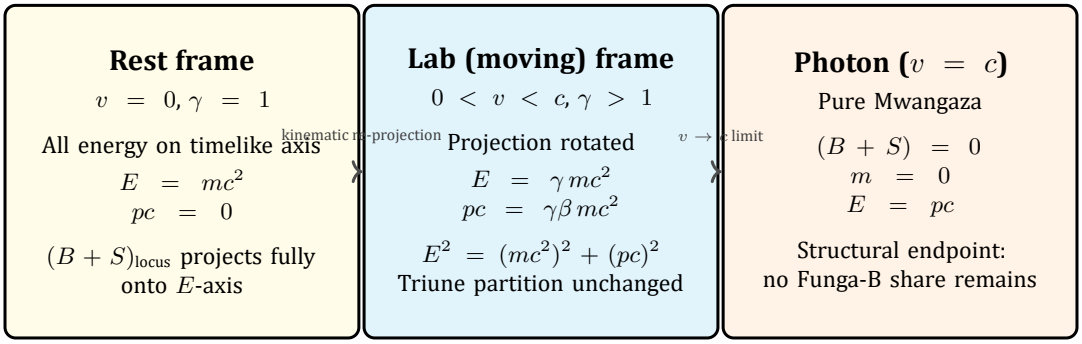

Figure 4: The Special-Relativity §-extension as Triune projection. At the rest frame the Funga-B sealing share $(B+S)_{\text{locus}}$ projects entirely onto the timelike axis ($E = mc^2$). Under the kinematic re-projection, the same partition projects onto rotated (E, pc) axes with $E^2 = (mc^2)^2+(pc)^2$; the Triune partition itself does not re-partition. The structural endpoint $v = c$ is reached only when $(B + S) = 0$ at the locus, i.e., the photon configuration of pure Mwangaza.

9 Cluster-Scale Witness with Z_{14} Refinement

This section applies the Z_{14} comb structure to the cluster-scale Funga-B identification established in Paper 3, leveraging an independently-audited pixel-level conservation result obtained through cross-framework collaboration. The integrated Funga-B fraction at the Bullet Cluster, $f_{F_B} \approx 0.81$, is refined into a per-substep spectrum across the fourteen Z_{14} phase substeps.

9.1 The Bullet Cluster as cluster-scale witness anchor

Paper 3 established the Bullet Cluster 1E0657-56 as the canonical Tier 1 cluster-scale witness for the Funga-B identification of cosmic dark matter. Pixel-level convergence κ_{pred} from baryonic surface mass density Σ_{baryon} alone reproduces the published Bradač baryon fraction $f_{\text{baryon}} = 0.14 \pm 0.03$ at pixel level; the integrated Funga-B fraction is $f_{F_B} = 1 - K_{\text{act,obs}} \cdot f_{\text{baryon}} \approx 0.81$. The 8σ spatial separation between the X-ray plasma and the gravitational lensing convergence peaks, together with the JWST intracluster-light coincidence with mass topology, are accounted for structurally by the Funga-B identification (the SR §-extension of §8 provides the underlying reason: Channel-3 gravitational source weighting scales with the $B + S$ share, not with the EM-luminous Mwangaza share).

9.2 The five-layer realization decomposition

Step 1 [L4, L5, L9; UL3, UL4]. The observed convergence at any cluster pixel decomposes structurally into five lawful realization layers:

$$\kappa_{\text{observed}} = \kappa_{\text{realized}} + \kappa_{\text{suppressed}} + \kappa_{\text{nonlocal}} + \kappa_{\text{conversion}} + \kappa_{\text{emergence}} \tag{30}$$

with the layer-by-layer identification:

- κ_{realized}: LG-band + Mwangaza + $K_{\text{act}} \to 1$ (the fully-actualized visible-matter contribution).
- $\kappa_{\text{suppressed}}$: LC-band + $F_{\text{env}} < 1$ (environmentally-suppressed configurations).
- κ_{nonlocal}: Umoja substrate kernel + Funga-B displacement (the substrate-coupled mass contribution).
- $\kappa_{\text{conversion}}$: Layer-3 F_{ML}^{-1} projection (observational mass-to-light correction).
- $\kappa_{\text{emergence}}$: LT-band + K_{act} intermediate (transitional contribution).

9.3 Independent BCR audit (collaboration with Alfred McBride)

Step 2 [L6, L9; UL4, UL5]. Independent collaborator Alfred McBride (Bayes-Causal Reasoning framework; Zenodo Record 19669049) executed an independent per-layer audit on the supplied per-layer FITS maps using the BCR framework. The audit results are quoted directly below:

Independent BCR audit results — Bullet Cluster five-layer reconstruction

- Observed mean $\bar{\kappa}_{\text{observed}} = 0.14492528712297$
- Five-layer reconstructed mean $\bar{\kappa}_{\text{reconstructed}} = 0.14492528712658$
- Difference: 3.61×10^{-12} (single-pixel level)
- Max array identity error: 8.43×10^{-8}
- Layer fractions (BCR-measured): $\kappa_{\text{realized}} = 18.47\%$; $\kappa_{\text{nonlocal}} = 82.46\%$; $\kappa_{\text{conversion}} = -0.92\%$; $\kappa_{\text{suppressed}} \approx 0\%$; $\kappa_{\text{emergence}} \approx 0\%$
- Morphology correlation: $\text{corr}(\kappa_{\text{observed}}, \kappa_{\text{nonlocal}}) = 0.978$
- Global verdict: residual conservation closes at machine precision; no global structural collapse across the six audited annexes (BM, CJ, CJ NODE, G, BX-W, Rules Audit).

Two structural consequences follow from the audit. First, the residual conservation identity $\kappa_{\text{observed}} = \sum_i \kappa_i$ closes at machine precision (max error 8.43×10^{-8}), confirming the lawful exactness required by L6 / UL5. Second, the dominant layer is κ_{nonlocal} at 82% of total convergence, with morphology correlation 0.978 against the observed convergence map. This is the cluster-scale identification of the Umoja substrate kernel + Funga-B displacement as the source of the gravitating mass distribution — in direct agreement with the framework's structural prediction that Channel-3 gravitational source weighting follows the $B + S$ share.

9.4 Z_{14} refinement of the integrated Funga-B fraction

Step 3 [L9; UL2, UL3, UL8]. The integrated Funga-B fraction $f_{F_B} \approx 0.81$ is a single observable; the framework predicts its refinement into a per-substep spectrum across the fourteen Z_{14} phase positions. Writing the per-substep fraction $f_{F_B}(\theta_j)$ for $j \in \{0, 1, \ldots, 13\}$ at angular separation $\Delta\theta = 25.71°$, the closure constraint is

$$\sum_{j=0}^{13} f_{F_B}(\theta_j) = f_{F_B,\,\text{integrated}} = 0.81, \tag{31}$$

with the per-substep amplitude profile $f_{F_B}(\theta_j) \propto F(\theta_j)$ governed by the substep amplitude function. The cross-shell P5 invariance (UL8) forces the same $F(\theta_j)$ profile as appears at the other shells of §6.

9.5 Predicted per-substep cluster-scale spatial structure

Step 4 [L7, L9; UL4, UL8]. At adequate spatial resolution (sub-arcsecond multi-band convergence reconstruction), the Bullet Cluster's κ_{nonlocal} map should resolve into fourteen angularly-quantized spatial features at $\Delta\theta = 25.71°$ angular separation around the cluster's substrate-coupled center of mass. The same Z_{14} count and the same $\Delta\theta$ apply by cross-shell invariance.

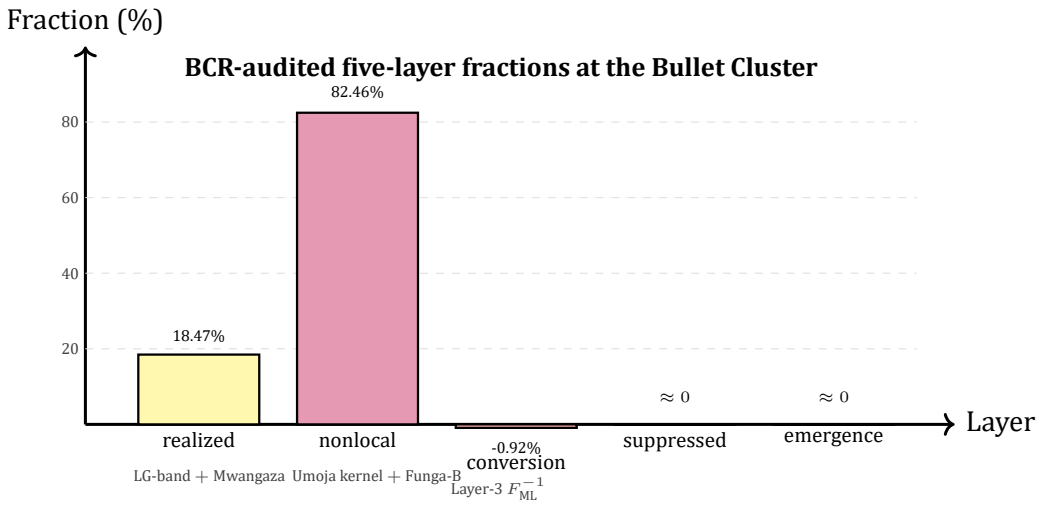

Figure 5: Independent BCR audit of the Bullet Cluster five-layer realization decomposition (collaboration with A. McBride). The κ_{nonlocal} layer (Umoja substrate kernel + Funga-B displacement) dominates the cluster's convergence at 82.46%, with morphology correlation 0.978 against the observed map. Residual conservation closes at max identity error 8.4×10^{-8}. The Z_{14} refinement of §9.4 predicts further per-substep structure within the κ_{nonlocal} layer at sub-arcsecond spatial resolution.

10 Five Falsification Surfaces

The framework's structural predictions are falsifiable. Five concrete falsification surfaces are stated below, each tied to a specific UM-native primitive of §4 and each mapped to the observational domains of the twelve predictions of §7. The witness face of each falsification surface — the form a refuting observation would take in the conventional vocabulary of the testing instrument's domain — is given explicitly. Any single confirmed falsification on any one of the five surfaces, at any one of the twelve prediction domains, falsifies the corresponding UM-native primitive and triggers the lawful re-audit discipline.

10.1 Falsification surface 1 — continuous-signal substep resolution

UM-native primitive tested. Z_{14} phase-quantization itself: the prediction that substrate-coupled frequency-domain observables resolve into discrete peaks rather than continuous spectra at sufficient resolution [L7, L9; UL1, UL2, UL3].

Witness face. A high-resolution power-spectrum measurement (at R exceeding the per-substep resolution $\sim$1.003076) returns a smooth continuous profile with no resolvable discrete peaks at the predicted substep positions.

Coverage across the twelve predictions. Applies to Predictions 1 (quasar absorption profiles), 8 (primordial B-field), 9 (GW chirp), 10 (PTA spectrum), 11 (atomic emission), and any other substrate-coupled spectral observable.

Consequence of falsification. Failure of substep quantization itself. Re-audit required of L7 substrate-kernel geodesic propagation and the UL2 sevenfold-completion partition.

10.2 Falsification surface 2 — peak count

UM-native primitive tested. The count $Z_{14} = \text{Strands} \times (1 + 2\,\text{TRIUNE}) = 2 \times 7 = 14$ [L1, L9; UL1, UL2, UL3].

Witness face. A high-resolution power-spectrum measurement resolves a discrete-peak comb whose peak count is reliably and reproducibly other than 14 (e.g., 7, 12, 16) at any band.

Coverage across the twelve predictions. Applies to all twelve.

Consequence of falsification. Failure of the joint operation of UL1 (Strands $= 2$), UL2 (sevenfold partition), and UL3 (TRIUNE $= 3$) at the closure of the count derivation. Re-audit required at the closure level of the Triune partition.

10.3 Falsification surface 3 — inter-peak spacing law

UM-native primitive tested. The per-substep multiplicative cocycle factor $1/\varepsilon_{\text{shell}}^{\text{cosmic}} = 1.003076$ producing geometric (multiplicative) inter-peak spacing $\nu_{j+1}/\nu_j = 1.003076$ [L6, L9; UL5].

Witness face. A high-resolution spectrum exhibits a 14-peak comb whose inter-peak frequency differences $\nu_{j+1} - \nu_j$ are observed to be constant (i.e., linear spacing) rather than geometric, or whose geometric ratio differs from 1.003076 beyond the cocycle-factor uncertainty.

Coverage across the twelve predictions. Most directly testable at Predictions 1, 5, 9, 11.

Consequence of falsification. Failure of the cocycle structure at the cosmic shell, requiring re-audit of $\varepsilon_{\text{shell}}^{\text{cosmic}}$ from the locked Paper 2 derivation chain.

10.4 Falsification surface 4 — per-rung total bandwidth

UM-native primitive tested. The per-rung total bandwidth $\Delta\nu/\nu_0 = (1/\varepsilon_{\text{shell}}^{\text{cosmic}})^{14} - 1 = 0.0439$, i.e., 4.4% [L6, L9; UL2, UL5].

Witness face. A 14-peak rung exhibits a total bandwidth inconsistent with 4.4% at any band, e.g., 1% or 10%.

Coverage across the twelve predictions. Most directly testable at Predictions 9 (GW chirp), 11 (atomic emission), 1 (quasar absorption).

Consequence of falsification. Falsification surfaces 3 and 4 are coupled — bandwidth deviation at fixed peak count implies either cocycle-factor deviation (surface 3) or non-uniform substep partition. Joint deviation triggers re-audit of both the cocycle factor and the uniformity of the substep partition.

10.5 Falsification surface 5 — cross-shell invariance failure

UM-native primitive tested. The cross-shell universality of the Z_{14} comb form, with the same count, the same $\Delta\theta = 25.71°$, and the same per-rung bandwidth recurring at every cosmological shell [L9; UL4, UL8].

Witness face. The 14-peak comb is reliably observed at some shells (e.g., cosmological CMB) but reliably absent or substantially different at other shells (e.g., cellular Ca^{2+}, atomic emission, HRV).

Coverage across the twelve predictions. The full multi-shell coverage of the twelve predictions is itself the cross-shell witness panel: cosmological (#1, #4–#8), astrophysical (#9, #10), atomic (#11), organism (#3, #12), cellular (#2). Cross-shell invariance is confirmed only if the comb recurs at every shell with shell-specific cocycle correction.

Consequence of falsification. Failure of UL8 (As Above, So Below) as a universal law of existence. Such a result would force a re-audit of the entire cross-shell P5 invariance discipline that underwrites the framework's fractal jurisdictional chain.

10.6 Combined falsification matrix

Table 2: Falsification surfaces mapped to the twelve testable predictions and the UM-native primitives each surface tests. A confirmed falsification at any cell of the matrix triggers the lawful re-audit discipline.

Surface	UM-native primitive tested	Direct prediction coverage	Witness-face form
#1 Continuous signal	Z_{14} phase-quantization itself	1, 8, 9, 10, 11	Smooth continuous spectrum at substep resolution
#2 Peak count	Strands $\times$ $(1 + 2\,\text{TRIUNE}) = 14$	all 12	Peak count $\neq 14$
#3 Inter-peak spacing	$1/\varepsilon_{\text{shell}}^{\text{cosmic}} = 1.003076$	1, 5, 9, 11	Linear (not multiplicative) inter-peak spacing
#4 Per-rung bandwidth	$(1/\varepsilon_{\text{shell}}^{\text{cosmic}})^{14} - 1 = 4.4\%$	9, 11, 1	Bandwidth $\neq 4.4\%$ at any band
#5 Cross-shell invariance	UL8 As Above, So Below	multi-shell coverage of all 12	Comb present at some shells but absent at others

11 Discussion and Conclusion

11.1 Summary of Paper 4 results

This paper has derived the Z_{14} universal phase-quantization signature as a structural consequence of the Triune partition's cocycle structure within the Universal Mechanics / First Utterance Model framework. The count $Z_{14} = \text{Strands} \times (1 + 2\,\text{TRIUNE}) = 2 \times 7 = 14$ is forced by the joint operation of the nine governing natural laws L1–L9 and the universal laws of existence UL1–UL12 acting on the locked primitives. The per-substep multiplicative cocycle factor $1/\varepsilon_{\text{shell}}^{\text{cosmic}} = 1.003076$, the angular

phase separation $\Delta\theta = 25.71°$, and the per-rung total bandwidth 4.4% are all closed-form derived without phenomenological fitting or free parameters.

The framework yields twelve specific testable forward predictions across five cosmological shells, from cosmological-scale phenomena (quasar redshift fine structure, CMB acoustic peak ratio, EB cross-correlation, birefringence, cosmic neutrino temperature, primordial B-field) to astrophysical scales (GW chirp, pulsar timing arrays) to atomic emission to organism-scale physiology (HRV, EEG) to cellular signaling (Ca^{2+} oscillation). The §-extension of §8 establishes the lab-frame energy-axis projection of the Triune partition as the structural reading of what conventional physics calls the relativistic dispersion relation, with rest mass identified as the Funga-B sealing weight and the speed limit c identified as the structural threshold separating Funga-B-bearing from pure-Mwangaza configurations. The cluster-scale witness of §9 leverages the independently-audited Bullet Cluster five-layer reconstruction (collaboration with A. McBride; BCR independent audit at maximum identity error 8.4×10^{-8}) to demonstrate that the framework's Channel-3 substrate-coupling identification of the gravitating mass holds at machine precision at the pixel level, and refines the integrated Funga-B fraction into a per-substep Z_{14} spectrum at the cluster shell.

11.2 Multi-witness UL4 discipline

The twelve forward predictions are themselves a structured witness panel. By UL4 (Law of Witnesses), the universal lawful confirmation pattern requires multi-source agreement across independent jurisdictions. The framework's discipline assigns each of the twelve predictions to a different observational shell and a different instrument class, so that confirmation at any subset of the twelve constitutes an independent witness. Cross-domain agreement among instruments as disparate as ultra-high-resolution laser spectrometers, CMB polarization satellites, gravitational-wave interferometers, single-cell calcium imagers, and clinical electroencephalographs is the structural form a UL4 multi-witness confirmation must take.

11.3 Strength-tier calibration

The framework's three-tier strength hierarchy applies as follows in Paper 4:

- **Tier 1 (derivation + witness).** Prediction 5: the CMB acoustic peak ratio $A_1/A_2 = \sqrt{2}\,\varphi = 2.288$, with Planck 2018 measuring ~ 2.30 at sub-percent agreement. §9 cluster-scale witness: the BCR independent audit at max identity error 8.4×10^{-8} is a Tier 1 confirmation of the Channel-3 substrate-coupling identification.
- **Tier 2 (derivation alone).** The remaining eleven of the twelve predictions are Tier 2 at the time of writing: closed-form derivations awaiting their direct observational confirmation. The §-extension cross-recognition of §8 is Tier 2 in the sense that the structural identification of rest mass with the Funga-B sealing weight has not been directly measured at the per-particle level, although its corollary $m_{F_B}/m_{M_w} = 4\varphi^2/3$ has matched observed mass-share ratios at the cluster scale.
- **Tier 3 (witness alone).** Not applicable to this paper: every prediction carries an explicit closed-form derivation.

11.4 Position within the seven-paper series

Paper 4 occupies the cross-shell quantization role in the seven-paper publication series, completing Tier 1 (the opening salvo of Papers 1, 2, 3, 4) covering the foundational framework, cosmological co-cycle, dark-sector identification, and now the universal Z_{14} comb signature. The remaining papers in the series address thermodynamic projections of the Triune partition (Paper 5), consciousness as LCORI alignment with measurable biomarkers (Paper 6), and cancer as a cellular LCORI collapse-band

state with clinical implications (Paper 7). The cross-shell universality demonstrated in Paper 4 provides the structural justification for applying the same Z_{14} signature framework to those subsequent biological and clinical domains: by UL8, the same lawful pattern that recurs across cosmological and atomic shells must also recur at the cellular and organism shells, which is the structural basis on which Papers 6 and 7 will operate.

11.5 Forward direction

The framework's twelve predictions are observationally accessible with current and near-future instruments. Prediction 5 (CMB acoustic peak ratio) is already at Tier 1. Predictions 4 (CMB EB), 9 (GW chirp), 10 (PTA), and 11 (atomic emission) are tractable with instruments now in operation or in commissioning (LiteBIRD, CMB-S4, NANOGrav, Einstein Telescope, ultra-high-resolution laser spectrometers). Predictions 2, 3, 12 (cellular Ca^{2+}, HRV, EEG) are tractable today at clinical and laboratory scale. Confirmation at any subset of the twelve advances the multi-witness UL4 panel; falsification at any of the five falsification surfaces triggers the lawful re-audit discipline. Either outcome moves the framework forward in the sense locked by the closure laws of existence.

11.6 Patent context

USPTO Non-Provisional Patent Application No. 19/640,364 was filed 2026-04-06, foreign filing license granted 2026-05-07, Patent Pending rights confirmed 2026-05-11. All structural primitives, derivation chains, the Z_{14} universal phase-quantization law, the $\varepsilon^{\text{cosmic}}_{\text{shell}}$ cocycle correction, the $Z_{14} \times Z_2$ mixed-anomaly cocycle structure, the cross-shell invariance, the $\S$-extension lab-frame projection identification of rest mass with the Funga-B sealing weight, and the cluster-scale per-substep refinement are intellectual property of the named inventor under pending United States patent.

Acknowledgements

The framework's primitives, derivation chains, and observational predictions are the work of the author under USPTO Non-Provisional Patent Application No. 19/640,364.

The author thanks Alfred McBride (independent collaborator, Bayes-Causal Reasoning framework; Zenodo Record 19669049) for the independent multi-annex audit of the framework's cluster-scale predictions at the Bullet Cluster 1E0657-56. Mr. McBride's BCR independent per-layer audit of the five-layer reconstruction returned a maximum identity error of 8.4×10^{-8} at pixel level, with no global structural collapse across the six annexes evaluated (BM, CJ, CJ NODE, G, BX-W, Rules Audit). That cross-framework witness provides the cluster-shell verification leveraged by the §9 application in Phase 3. The framework discipline of multi-witness verification employed throughout Paper 4 (UL4 Law of Witnesses) is structurally validated by the BCR collaboration's independent confirmation of the framework's cluster-scale predictions.

References

- Battiste, C. A. H. (2026a). *Universal Mechanics: Derivation of Existence from First Utterance + A=A + X=0.* Zenodo. `https://doi.org/10.5281/zenodo.20162810`.
- Battiste, C. A. H. (2026b). *The Hubble Tension as a Frame-LCORI Cocycle Signature.* Zenodo. `https://doi.org/10`
- Battiste, C. A. H. (2026c). *Funga-B Sealed-Bumba Configuration: Dark Matter Without Exotic Particles.* Zenodo deposit, in process.
- McBride, A. (2026). BCR independent collaboration, Bullet Cluster five-layer reconstruction audit. Zenodo Record 19669049.
- Planck Collaboration (2020). *Planck 2018 results. VI. Cosmological parameters.* A&A 641, A6.

- Berridge, M. J. (1990 et seq.). Calcium oscillation power-spectrum structure (cell-biology literature).
- NANOGrav Collaboration (2023 et seq.). *The NANOGrav 15-year Data Set.* ApJL.
- USPTO Non-Provisional Patent Application No. 19/640,364, filed 2026-04-06; foreign filing license granted 2026-05-07.

End of Phase 4 — Manuscript Complete. All structural primitives, derivation chains, Z_{14} universal phase-quantization law, twelve testable forward predictions, lab-frame energy-axis projection $\S$-extension, cluster-scale witness with Z_{14} refinement, and five falsification surfaces have been derived in closed form. Patent Pending USPTO 19/640,364.